Faraday Discussions

Ultrafast Branching in Intersystem Crossing Dynamics Revealed by Coherent Vibrational Wavepacket Motions in a Bimetallic Pt(II) Complex

Journal:	*Faraday Discussions*
Manuscript ID	FD-ART-01-2022-000009.R1
Article Type:	Paper
Date Submitted by the Author:	02-Feb-2022
Complete List of Authors:	Kim, Pyosang; Northwestern University, Chemistry; Argonne National Laboratory, Chemical Science and Engineering Division Valentine, Andrew; University of Washington, Department of Chemistry Roy, Subhangi; North Carolina State University, Department of Chemistry Mills, Alexis; University of Washington, Department of Chemistry Castellano, Felix; North Carolina State University, Department of Chemistry Li, Xiaosong; Department of Chemistry, University of Washington, Chen, Lin; Northwestern University, Chemistry; Argonne National Laboratory, Chemical Sciences and Engineering

Ultrafast Branching in Intersystem Crossing Dynamics Revealed by Coherent Vibrational Wavepacket Motions in a Bimetallic Pt(II) Complex

Pyosang Kim,[*,1,2] Andrew J. S. Valentine,[3] Subhangi Roy,[4] Alexis W. Mills,[3] Felix N. Castellano,[*,4] Xiaosong Li,[*,3] and Lin X. Chen[*,1,2]

[1]Department of Chemistry, Northwestern University, Evanston, Illinois 60208, United States

[2]Chemical Science and Engineering Division, Argonne National Laboratory, Lemont, Illinois 60349, United States

[3]Department of Chemistry, University of Washington, Seattle, Washington 98195, United States

[4]Department of Chemistry, North Carolina State University, Raleigh, North Carolina 27695-8204, United States

Abstract

Ultrafast excited-state processes of transition metal complexes (TMCs) are governed by complicated interplays between electronic and nuclear dynamics, which demand a detailed understanding to achieve optimal functionalities of photoactive TMC-based materials for many applications. In this work, we investigated a cyclometalated platinum(II) dimer known to undergo a Pt-Pt bond contraction in metal-metal-to-ligand-charge-transfer (MMLCT) excited state using femtosecond broadband transient absorption (fs-BBTA) spectroscopy in combination with geometry optimization and normal mode calculations. Using sub-20 fs pump and broadband probe pulses in fs-BBTA spectroscopy, we are able to correlate coherent vibrational wavepacket (CVWP) evolution with stimulated emission (SE) dynamics of the ^{1}MMLCT state. The results demonstrated that the 145 cm^{-1} CVWP motions with the damping times of ~ 0.9 ps and ~ 2 ps originate from coherent Pt-Pt stretching vibrations in the singlet and triplet MMLCT states, respectively. On the basis of excited-state potential energy surface calculations in our previous work, we rationalized that the CVWP transfer from Franck-Condon (FC) state to the ^{3}MMLCT state was mediated by a triplet ligand-centered (^{3}LC) intermediate state through two step intersystem crossing (ISC) on a time scale shorter than a period of the Pt-Pt stretching wavepacket motions. Moreover, it was found that the CVWP motion with 110 cm^{-1} frequency decays with the damping time of ~ 0.2 ps, well matching the time constant of 0.253 ps corresponding to a redshift in the SE feature at early time. This observation indicates that the Pt-Pt bond contraction changes the stretching frequency from 110 to 145 cm^{-1} and stabilize the ^{1}MMLCT state relative to the ^{3}LC state with the ~ 0.2 ps time scale. Thus, the ultrafast ISC from the ^{1}MMLCT to the ^{3}LC states occurs before the Pt-Pt bond shortening. The findings herein provide insight into understanding the impact of Pt-Pt bond contraction on ultrafast branching of the ^{1}MMLCT population into the direct (^{1}MMLCT $\rightarrow$ ^{3}MMLCT) and indirect ISC pathways (^{1}MMLCT $\rightarrow$ ^{3}LC $\rightarrow$ ^{3}MMLCT) in the Pt(II) dimer. These results revealed intricate excited state electronic and nuclear motions that could steer the reaction pathways with levels of details that have not achieved before.

Introduction

Transition metal complexes (TMCs) have received tremendous attentions in solar energy conversion, photocatalysis and optoelectronics due to their versatile photochemical properties enabling a variety of functions as electron donor/acceptor, photoluminescence emitters, and redox/catalytic centers.[1-8] Recent advances in femtosecond optical and X-ray spectroscopy/scattering have brought new insight into electronic and nuclear dynamics of excited-state TMCs in ultrafast time regime.[9-16] The studies have shown that electronic transition induced by light and nuclear motions may occur on similar time scales along the excited state trajectories. The observations indicate that the nuclear and electronic coordinates are coupled, and the excited state trajectories could go across multiple potential energy surfaces (PESs) before relaxation to vibrational equilibrium. Therefore, a precise understanding of the interplay between nuclear and electronic degrees of freedom in ultrafast regime is particularly crucial in the development of advanced TMC-based materials for aforementioned applications.

Cyclometalated platinum(II) dimer complexes offer an ideal platform to investigate the interplay of electronic and nuclear dynamics in TMCs, because they display distinct structural changes in the excited-state upon the electronic transitions, and their structural dynamics have been linked to their emission properties as phosphorescence emitters in organic light-emitting diodes (OLEDs).[8, 17] Previous experimental and theoretical studies on these systems have revealed strong structural dependent photophysical properties, which enable tunability in their absorption/emission properties via chemical synthesis such as changing the Pt-Pt bond distance. As the Pt-Pt distance decreases, the interaction between the $5d_{z^2}$ orbitals of the two Pt(II) atoms becomes stronger, and the energy splitting between the Pt – Pt σ bonding and σ^* antibonding molecular orbitals (MOs) increases as shown in Figure 1a. Since the close Pt-Pt distance can raise the energy of the σ^* antibonding MO higher than other d orbitals, the lowest electronic transition transforms from a localized ligand-centered (LC) and/or a metal-to-ligand-charge transfer (MLCT) in one half of the molecule with a pseudo two-fold symmetry to a delocalized metal-metal-to-

ligand-charge transfer (MMLCT).[18-23] This transformation from the LC/MLCT to the MMLCT transitions results in a concomitant redshift in absorption and phosphorescence spectra. Moreover, the MMLCT excitation moves an electron from the σ^* antibonding MO to the π^* MO of cyclometalating ligands, thereby increasing the Pt–Pt bond order by ~ 0.5 due to the removal of the antibonding electron, and resulting in a significant Pt–Pt bond contraction in the excited-state. Indeed, the photoinduced Pt-Pt bond shrinkage has been observed in the triplet MMLCT state through X-ray transient absorption and scattering experiments.[24, 25]

Although the Pt-Pt bond contraction has been known as the primary structural change in the MMLCT excited-state of the Pt(II) dimers, a question remains on how the Pt-Pt bond shortening directly affect the excited-state processes including intersystem crossing (ISC) to the ^{3}MMLCT state. To address the question, our previous works utilized optical transient absorption spectroscopy equipped with ~ 35 fs pump pulse to create coherent vibrational wavepacket (CVWP) motions and track their evolution along the excited-state trajectories. Upon the photoexcitation of ^{1}MMLCT state, we have observed a strong beating signal corresponding to Pt-Pt stretching CVWP motions in pyrazolate-, 2-thiolpyridyl- and 2-hydroxypyridyl-bridged Pt(II) dimers.[13, 26, 27] Furthermore, a comparative study on the Pt-Pt stretching CVWP dynamics have been conducted in a series of structurally related 2-hydroxypyridyl-bridged Pt(II) dimer. We found that the Pt-Pt stretching CVWP generated in Franck-Condon (FC) region can be sustained during the ISC by adding phenyl substituents on the bridging ligands. With the help of quantum mechanical calculations of excited-state PESs, it was shown that the interaction between the phenyl rings and Pt(II) atoms stabilizes the energy of ^{1}MMLCT state relative to a ^{3}LC state and thus locates the ^{3}LC states in the vicinity of FC state. Thus, ultrafast ISC can take place from the ^{1}MMLCT to the ^{3}LC intermediate state followed by subsequent internal conversion (IC) to the ^{3}MMLCT state. However, determining the population decays of the ^{1}MMCLT state and corresponding CVWP dynamics was difficult in the previous study, largely due to the lack of stimulated emission (SE) features in the probe spectrum (520 – 700 nm) used in the TA measurements. Hence, it is still unclear how the photoinduced Pt-Pt contraction modulates the energy of ^{1}MMLCT state relative to the ^{3}LC state beyond the FC region and then affect the ultrafast ISC pathway.

Using femtosecond broadband transient absorption spectroscopy (fs-BBTA), the work presented herein investigated the CVWP dynamics during the ISC processes in one of 2-hydroxypyridyl-bridged Pt(II) dimers that showed the long-lived vibrational coherence in our previous study (inset in Figure 1b). The broadband probe spectrum covering the range of 520 – 850 nm enabled us to clearly identify the SE dynamics and relevant CVWP motions appearing in 600 - 850 nm. Also, sub-20 fs pump pulses enhance the amplitude of CVWP motions associated with the photoinduced structural changes including the Pt-Pt contraction as compared to the previous measurements as the synchronization of the CVWP motion improves. By correlating the temporal evolution of SE and CVWP signals, we demonstrate two intriguing facts of ISC processes in the Pt(II) dimer; 1) the initially populated MMLCT state branches into the direct (^{1}MMLCT $\rightarrow$ ^{3}MMLCT) and indirect ISC path (^{1}MMLCT $\rightarrow$ ^{3}LC $\rightarrow$ ^{3}MMLCT) and 2) the ultrafast branching occurs before completing the Pt-Pt bond contraction on the ~ 0.2 ps time scale. Therefore, the photoinduced Pt-Pt contraction is a key structural factor to determine the ultrafast ISC and the CVWP transfer in the vicinity of the FC region.

Experimental Section

Sample Preparation. The Pt(II) dimer was synthesized and structurally characterized as described in our previous publication.[28]

Steady-State Measurements. Steady-state absorption and emission spectra were measured by Shimadzu UV-3600 UV-Vis-NIR spectrophotometer and Horiba Scientific model Fluorolog-3 spectrometer, respectively. Both measurements were performed in 1 cm pathlength quartz cuvettes in THF at room temperature.

Femtosecond Broadband Transient Absorption Spectroscopy. For the fs-BBTA measurements, a Yb:KGW regenerative amplifier (Light Conversion, Pharos-10W) was used to generate 1030 nm fundamental pulses at 10 kHz repetition rate with a pulse width of 160 fs. The fundamental beam was split into two pulses using 90/10 beam splitter for generation of a visible pump and a broadband probe pulse. The former is accomplished by a home-built noncollinear optical parametric amplifier (NOPA) for the pump pulses centered at 540 nm with 60 nm bandwidth.[29] The pump pulses were compressed with a chirped mirror pair (Laser Quantum, DCM-12) and a fused silica wedge pair (Newport) to 17.5 fs full width at half maximum (FWHM) at the sample

position, which was characterized by a second-harmonic generation frequency-resolved optical gating (SHG-FROG) with a 5 μm thick Beta Barium Borate (BBO) crystal (United Crystals Inc.) (Figure S1). For broadband probe, the low-power beams were focused on a 3 mm thick YAG window (EKSMA) by a 10 cm plano-convex lens to generate white light continuum (WLC) covering 520 – 850 nm range. The WLC was subsequently compressed by a chirped mirror pair (Laser Quantum, DCM-9). The pump and probe beams were focused on the sample contained in a 1 mm pathlength quartz cuvette using a 25 cm concave mirror. The optical time delay between pump and probe pulses was controlled by a motorized linear stage (Newport, XMS160-S). To measure the TA spectra, the "pump-on" and "pump-off" probe spectra were obtained by a chopper operating at 500 Hz and detected with a spectrometer (Andor, Kymera 328i) and a sCMOS camera (Andor, Zyla-5.5). The TA measurements were carried out with the pump polarization in a magic angle (54.7°) with respect to the probe polarization to prevent polarization-dependent signals.

Quantum Mechanical Calculations. All calculations were performed at University of Washington using GAUSSIAN16.[30] The 6-31g(d) basis set was employed for all light atoms, while the LanL2DZ effective core potential and associated basis set[31] was used for Pt atoms. Density functional calculations were performed with the ωB97X-D functional.[32] This functional was chosen because it is range-separated, to better describe charge-transfer excited states,[33] and it contains dispersion corrections, necessary to capture π-π interactions.[32] Excited states were evaluated using time-dependent density functional theory (TD-DFT). Energetic minima found by ground- and excited-state geometry optimizations were confirmed by normal mode calculations at the same level of theory.

Results and Discussion

Excited-State Dynamics. The steady-state absorption and emission spectra of Pt(II) dimer are depicted in Figure 1b. In the previous report by Chakraborty et al., three electronic transition bands were confirmed by TD-DFT calculations: 1) ^{1}LC band below 350 nm, 2) a mixture of ^{1}LC and ^{1}MLCT bands in 350 – 450 nm range and 3) ^{1}MMLCT bands above 450 nm.[28] This work also assigned the broad emission spectrum around 780 nm to the ^{3}MMLCT band.

We performed the fs-BBTA measurements to identify the excited-state dynamics associated with the ISC from the singlet to the triplet MMLCT state upon the photoexcitation in the 500 – 590 nm pump spectral range (Figure 1c). To get details of the excited-state dynamics for the Pt(II) dimer, the global kinetic analysis was carried out on the BBTA data scanned up to 150 ps using Glotaran program[34] as given in Figure 1d. The best fits to the TA kinetics have four time constants of 0.253, 1.25, 4.18 and 90.3 ps and a constant offset originating from the 55.9 ns decay of the ^{3}MMLCT state.[28] The evolution-associated difference spectra (EADS) for the time

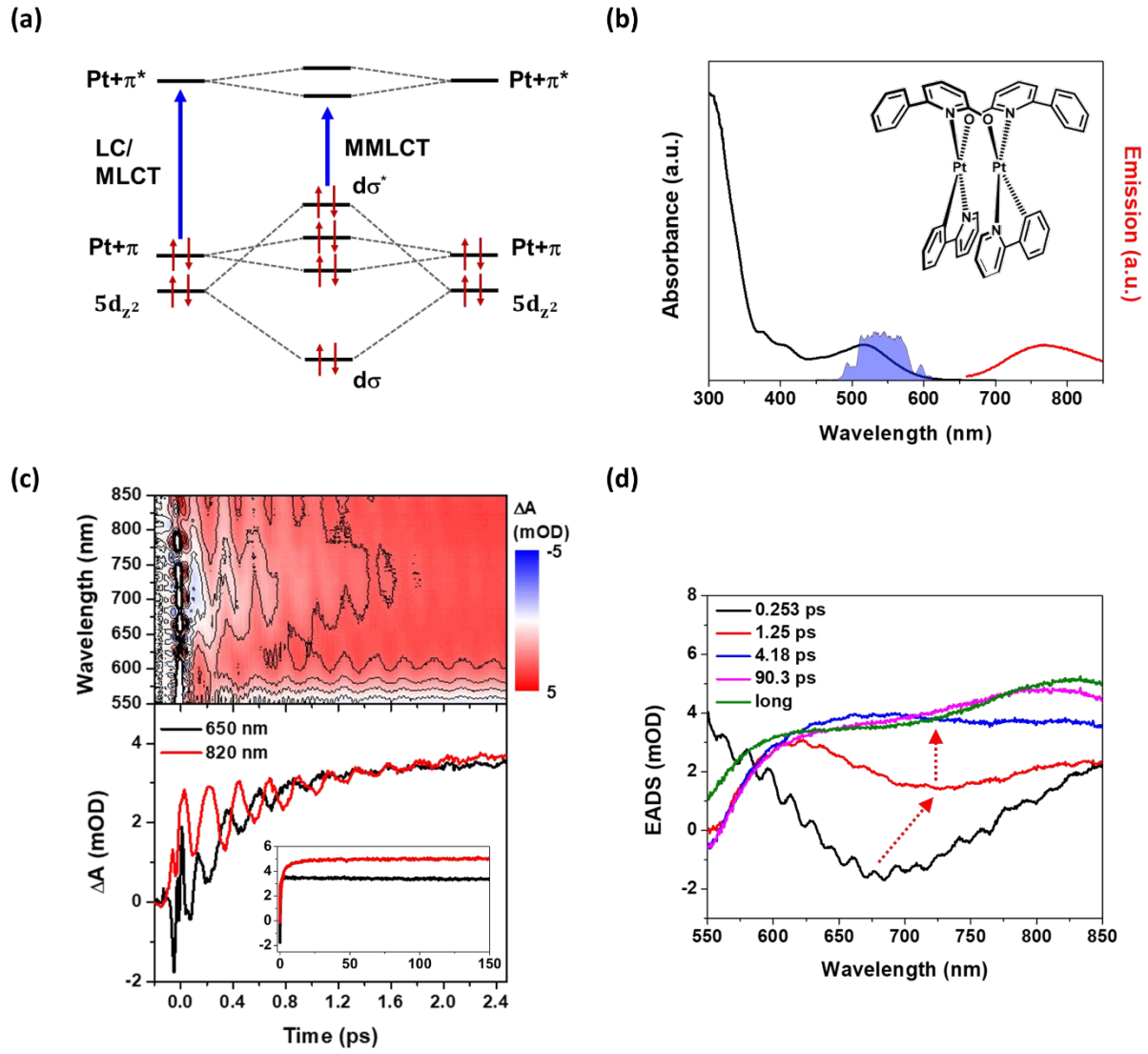

Figure 1. (a) Molecular orbital energy scheme for Pt(II) dimer, illustrating the interaction between the $5d_{z^2}$ orbitals of Pt(II) atoms and its impact on the transformation of lowest electronic transition from LC/MLCT to MMLCT. (b) steady-state absorption (black) and emission spectra (red) for Pt(II) dimer in THF and the pump pulse spectrum (blue) used in the fs-BBTA. The inset shows schematic molecular structure of Pt(II) dimer. (c) the fs-BBTA data map (top) and the kinetic traces (bottom) at 650 and 820 nm probe wavelengths. The inset exhibits the TA kinetic traces up to 150 ps delay at the same probe wavelengths. (d) Evolution-associated difference spectra (EADS) obtained by the global kinetic analysis of fs-BBTA data scanned with time delays of 150 ps. The red dotted arrows highlight the decay dynamics of SE signal.

component of 0.253 ps clearly shows the stimulated emission (SE) feature emerging between the edge of the ^{1}MMLCT absorption (~ 600 nm) and the peak of the ^{3}MMLCT emission (770 nm). When converted to the 1.25 ps EADS, the SE signal decays with a redshift to ~725 nm and a concomitant growth of ESA signal around 625 nm. Then, the SE feature is completely quenched

in the 4.18 ps EADS, leading to the further growth of the excited-state absorption (ESA) signals in 625 – 850 nm. Finally, the 4.18 and 90.3 ps EADSs display the rise of ESA features around 825 nm. Although the ^{1}MMLCT fluorescence was not detected in the steady-state measurement, the SE kinetics can be reasonably connected to the quenching dynamics of the initially populated ^{1}MMLCT state. In particular, since the SE decay dynamics does not accompany with the recovery of ground-state absorption (GSB) signal around 550 nm and the decay of ESA signal, we determined the ISC rates from the singlet to triplet MMLCT state to be 1.25 ps. The origin of the SE dynamics on 0.253 ps time scale will be discussed later. Based on the previous TA study of pyrazolate-bridged Pt(II) dimers,[23] the slower two components, 4.18 and 90.3 ps, are herein assigned to intramolecular vibrational redistributions (IVR) and vibrational cooling occurring in the ^{3}MMLCT manifold.

Coherent Vibrational Wavepacket Dynamics. The ultrashort pump pulse (17.5 fs) used in the fs-BBTA measurement launched CVWPs modulating the BBTA signals as a function of the pump – probe delay shown in Figure 1c. To identify the frequencies associated with the CVWP motions, we performed fast Fourier transformation (FFT) on the oscillatory residuals extracted from the global kinetic analysis of the BBTA data. In Figure 2a, wavelength-resolved FFT power map obtained by the FFT of the oscillations in the delay time window of 0.1-2.5 ps show a dominating peak at 145 cm^{-1}, centered around 580, 700 and 840 nm. The broadband probe enabled us to measure newly the 145 cm^{-1} CVWP motions around 840 nm in comparison to our previous study in which this probe wavelength was inaccessible.[27] Three minor peaks were also observed at 110, 228 and 292 cm^{-1} except the 914 cm^{-1} Raman mode of THF solvent.[35] The FFT map displays a decrease of amplitude at ~ 650 and ~ 750 nm, indicating a π phase change, the so-called "node", in the 145 cm^{-1} CVWP motions. As shown in Figure 2b, wavelength-resolved residual map clearly shows the spectral positions of the nodes and their temporal evolution along the probe wavelength. For the node at ~ 650 nm in the FFT map, it appears at 600 nm from ~ 0.3 ps and then moves to 650 nm. Similarly, the other node transforms from 675 nm to 770 nm. The CVWP motions created in the PES show the phase shift of the oscillations at the minimum of the PES, resulting in the zero-amplitude node as shown in Figure 2.[36-38] Therefore, the spectral position of the node can be a strong evidence for the origin of the CVWP; the ground-state wavepacket produces the node around the absorption (GSB) maximum, while the node of the excited-state wavepacket arises near the fluorescence (SE) or ESA maximum.[39] The two nodes observed in the 145 cm^{-1} CVWP motions

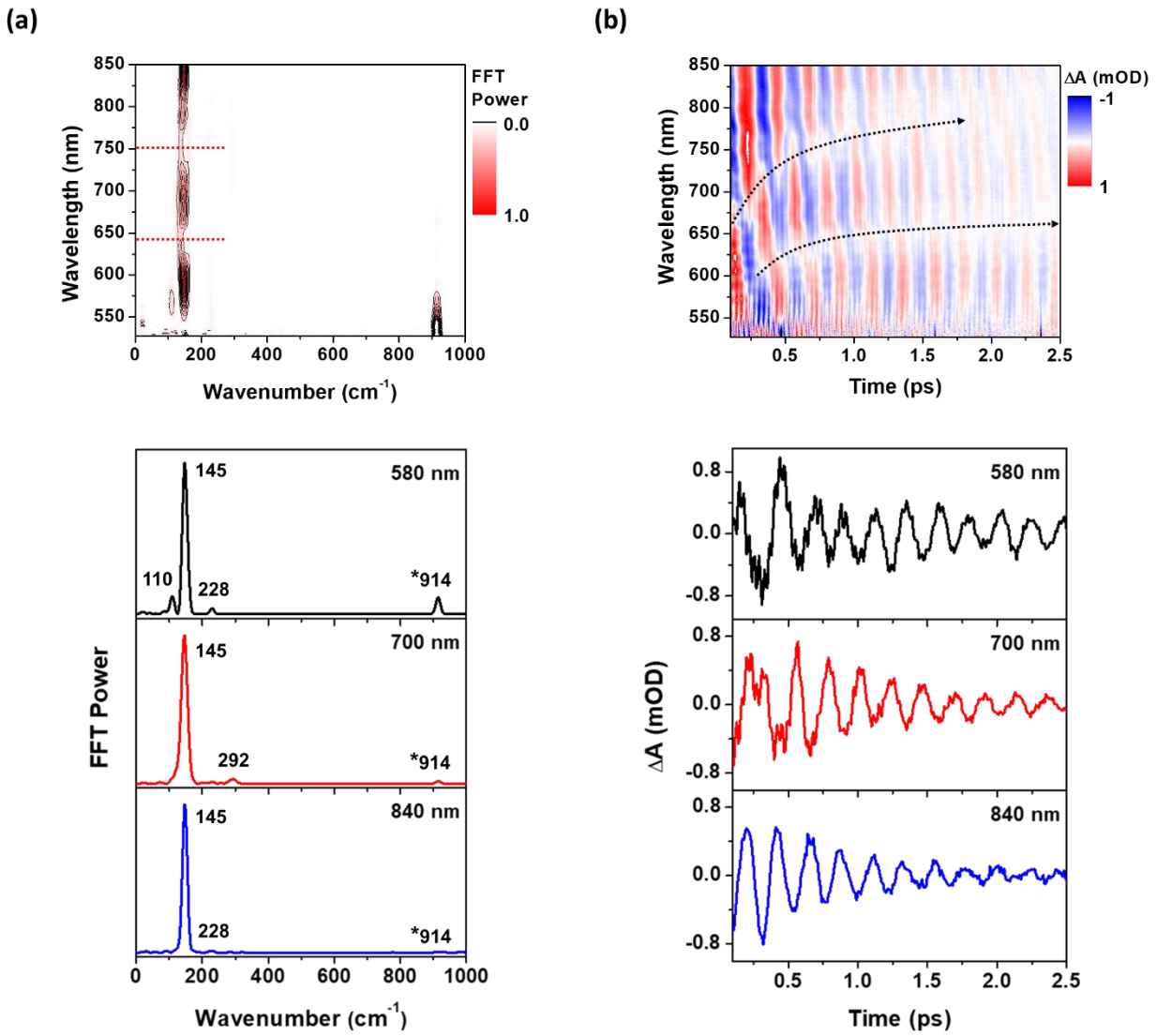

Figure 2. (a) Wavelength-resolved FFT power map (top) and FFT spectra (bottom) at 580, 700 and 840 nm. The FFT was performed on the oscillations in 0.1 – 2.5 ps window along the probe wavelength. The oscillatory residuals in 0 – 0.1 ps window were truncated to avoid the contribution of cross-phase modulation to the FFT. The red dotted lines in the FFT map indicate the node positions that the π phase jump occur. (b) wavelength-resolved residual map (top) and oscillatory signals at 580, 700 and 840 nm. The dotted arrows highlight the node shift along the time delay.

emerge beyond the ground-state absorption region (500 – 600 nm, Figure 1b). Thus, the 145 cm^{-1} CVWP motions are expected to be the excited-state wavepackets. In particular, the node shift from 675 to 770 nm shown in the residual map occurs near the SE maxima of the 0.253 and 1.25 ps

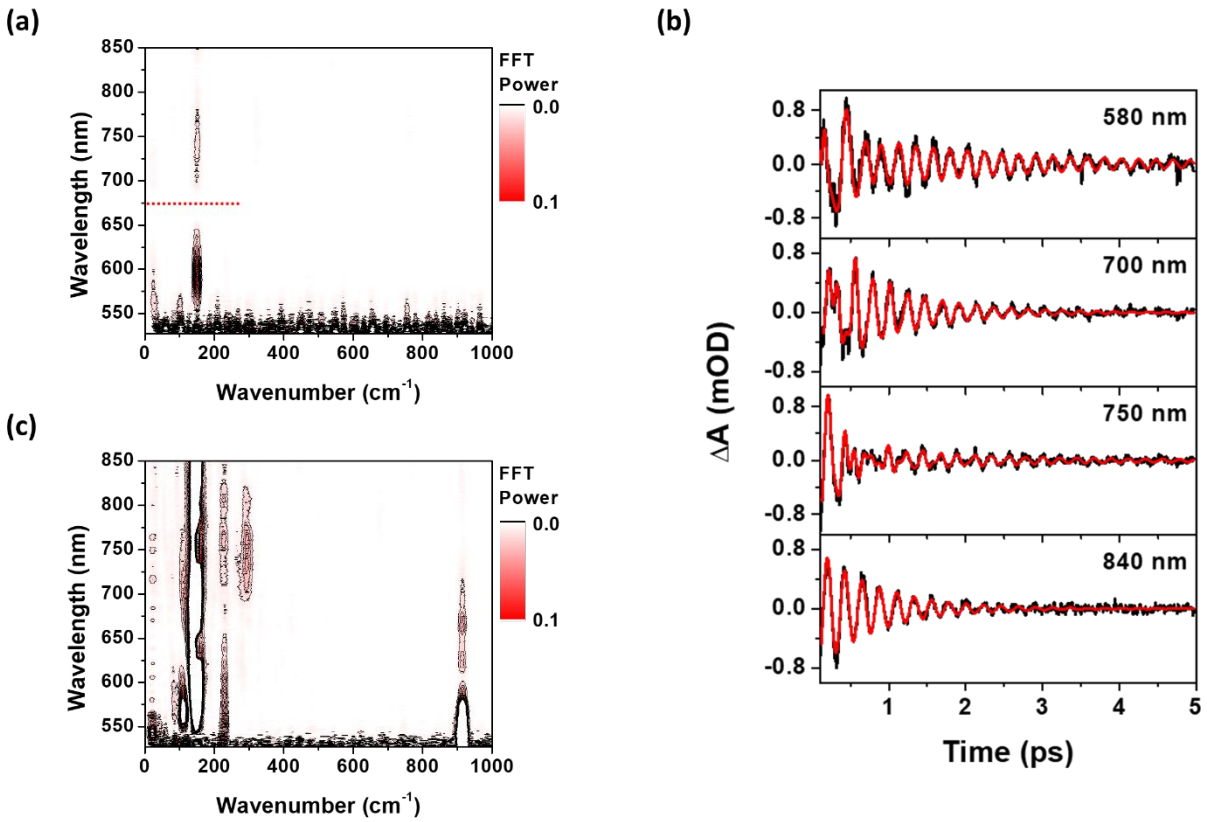

Figure 3. (a) Wavelength-resolved FFT power map obtained by the FFT on the oscillations in the time window of 2.5 – 5ps. The red dotted line indicates the spectral position of the node. (b) the oscillatory residuals (black) with the fit to exponentially damped sine functions (red) at 580, 700, 750 and 840 nm. (c) Zoom in the FFT power map of the oscillations in 0.1 – 2.5 ps window to clearly show the amplitude distribution of 110, 228 and 292 cm^{-1} frequencies.

EADS (Figure 1d), indicating that the 145 cm^{-1} CVWP motions generating the node at ~ 750 nm in the FFT map originate from the ^{1}MMLCT state.

The oscillatory residuals in the time window of 2.5 – 5 ps was FFT-analyzed separately in order to investigate the spectral positions of the two nodes beyond 2.5 ps delay (Figure 3a). In comparison with the wavelength-resolved FFT map in 0.1 – 2.5 ps window (Figure 2b), the FFT map in 2.5 – 5 ps window clearly shows an absence of the node around 750 nm, while the node around 650 nm is slightly redshifted to ~ 675 nm and preserved over 2.5 ps. The damping times of the oscillations near 580, 700, 750 and 840 nm were fitted to a combination of sines multiplied by exponential functions (Figure 3b). The results are summarized in Table 1. The 145 cm^{-1} CVWPs detected around 580 and 750 nm show a very long dephasing time of ~ 2 ps, while the one around

Table 1. Dephasing Times of Oscillations at 580, 700, 750 and 840 nm

Parameter	580 nm	700 nm	750 nm	840 nm
τ_1 (145 cm^{-1})	2.35 ± 0.18 ps	0.95 ± 0.04 ps	0.23 ± 0.01 ps 2.11 ± 0.28 ps	0.78 ± 0.02 ps
τ_2 (228 cm^{-1})	0.58 ± 0.30 ps	0.63 ± 0.14 ps	0.75 ± 0.10 ps	–
τ_3 (292 cm^{-1})	–	0.44 ± 0.05 ps	0.68 ± 0.08 ps	–
τ_4 (110 cm^{-1})	0.24 ± 0.02 ps	0.16 ± 0.01 ps	–	–

700 and 840 nm exhibits the damping time of ~ 0.9 ps. This fit explains that the beating node near 750 nm vanishes twice as fast as the other observed around 650 nm. Therefore, the temporal change of FFT map for the 145 cm^{-1} CVWPs suggests the two nodes near 650 nm and 750 nm correspond to the different excited-states, respectively. As was already mentioned, the node shift from 675 to 770 nm well matches to the redshift of SE signals (Figure 1d). Also, the damping times of ~ 0.9 ps indicates the 145 cm^{-1} CVWP motions at 700 and 840 nm decay within the ISC rate of 1.25 ps. Both findings justify that the node at ~ 750 nm stems from the ^{1}MMLCT state. Contrarily, the node at ~ 650 nm persists over the ISC rate. Furthermore, the node shift from 650 to 675 nm seems to be largely due to the growth of ESA feature induced by the quenching of SE signals as shown in the transition from 1.25 ps to 4.18 ps EADSs (Figure 1d). Thus, the 145 cm^{-1} CVWP motions generating the node around 650 nm can be reasonably assigned to the nuclear motions populated in the ^{3}MMLCT state.

The lower frequency mode, 110 cm^{-1} CVWP, has been observed for the same Pt(II) dimer in our previous work.[27] The other ultrafast TA studies have shown also the similar frequency in the pyrazolate- and 2-thiolpyridyl-bridged Pt(II) dimers equipped with the same cyclometalating ligands.[26, 40] Since the lower frequency oscillation had a strong amplitude mainly near the ground-state absorption region, the previous studies reported that its origin is the ground-state wavepacket. Although the current fs-BBTA measurement also showed the similar trend, the damping time of this oscillation suggests a possibility of the excited-state wavepacket. In general, the ground-state CVWP has long-lived coherence lifetime compared to the excited-state CVWP, because the ground-state wavepacket do not undergo electronic transitions, vibrational relaxations, solvent-

related reorganization and photoinduced structural changes, strongly affecting the vibrational dephasing. Very surprisingly, the 110 cm^{-1} oscillation at 580 nm for the Pt(II) dimer decays 5- 10 times faster than the 145 cm^{-1} excited-state CVWP. The damping time of 0.24 ps is in good agreement with the 0.253 ps time scale corresponding to the redshift of the SE features. Moreover, the current fs-BBTA clearly unraveled that the CVWP motions near 700 nm contain the 110 cm^{-1} vibration as shown in Figure 3a and the oscillatory fit showed the damping time of 0.16 ps, supporting the 110 cm^{-1} CVWP is highly possibly the excited-state wavepacket.

The 228 and 292 cm^{-1} frequency vibrations are observed beyond the ground state absorption region (Figure 3c). Also, the oscillatory fit results show their damping times are 0.6 – 0.8 ps. Although it is hard to determine the spectral position of the node for these vibrations in the FFT map due to the weak amplitudes, their vibrational dephasings exhibit similar time scales to the damping time of 145 cm^{-1} CVWP at 700 and 840 nm, suggesting that these nuclear motions originate from the ^{1}MMLCT state and depahse during the ISC with the rate of 1.25 ps.

Nuclear Motions Associated with Photoinduced Structural Changes. To assess the correlation between the photoinduced nuclear reorganization and the observed CVWP dynamics, the structure optimization and the normal mode calculations were performed as pictured in Figure 4. The optimized molecular geometries of the ^{1}MMLCT and ^{3}MMLCT states show significant changes from the one of the ground-state in terms of Pt-Pt bond distance and dihedral angle of two planes of cyclometalating ligands: 1) the Pt-Pt bond is shortened from 2.94 Å in the ground-state to 2.70 Å and 2.69 Å in the singlet and triplet MMLCT states, 2) the distance between the ligand planes is decreased from 3.47 Å in the ground-state to 3.20 Å and 3.22 Å in the singlet and triplet MMLCT states, 3) the twisting angle is reduced from 15.06° in the ground-state to 11.01° and 11.31° in the singlet and triplet MMLCT states. In particular, the bond contraction in the MMLCT states has been directly observed by the X-ray transient absorption and scattering measurements of the structurally related pyrazole-bridged Pt(II) dimers.[24, 25, 41]

In Figure 4b, the normal mode calculations of the ground-state showed the Pt-Pt stretching vibration at 114.7 cm^{-1} frequency. For the ^{1}MMLCT and ^{3}MMLCT states, the Pt-Pt stretching vibrations were also found at 149.7 and 145.5 cm^{-1} frequencies in the computations. The Pt-Pt stretching frequency is upshifted in the excited MMLCT states because the Pt-Pt bond order increases by 0.5 due to the lack of one electron in the antibonding $d\sigma^{*}$ orbital. The calculated Pt-

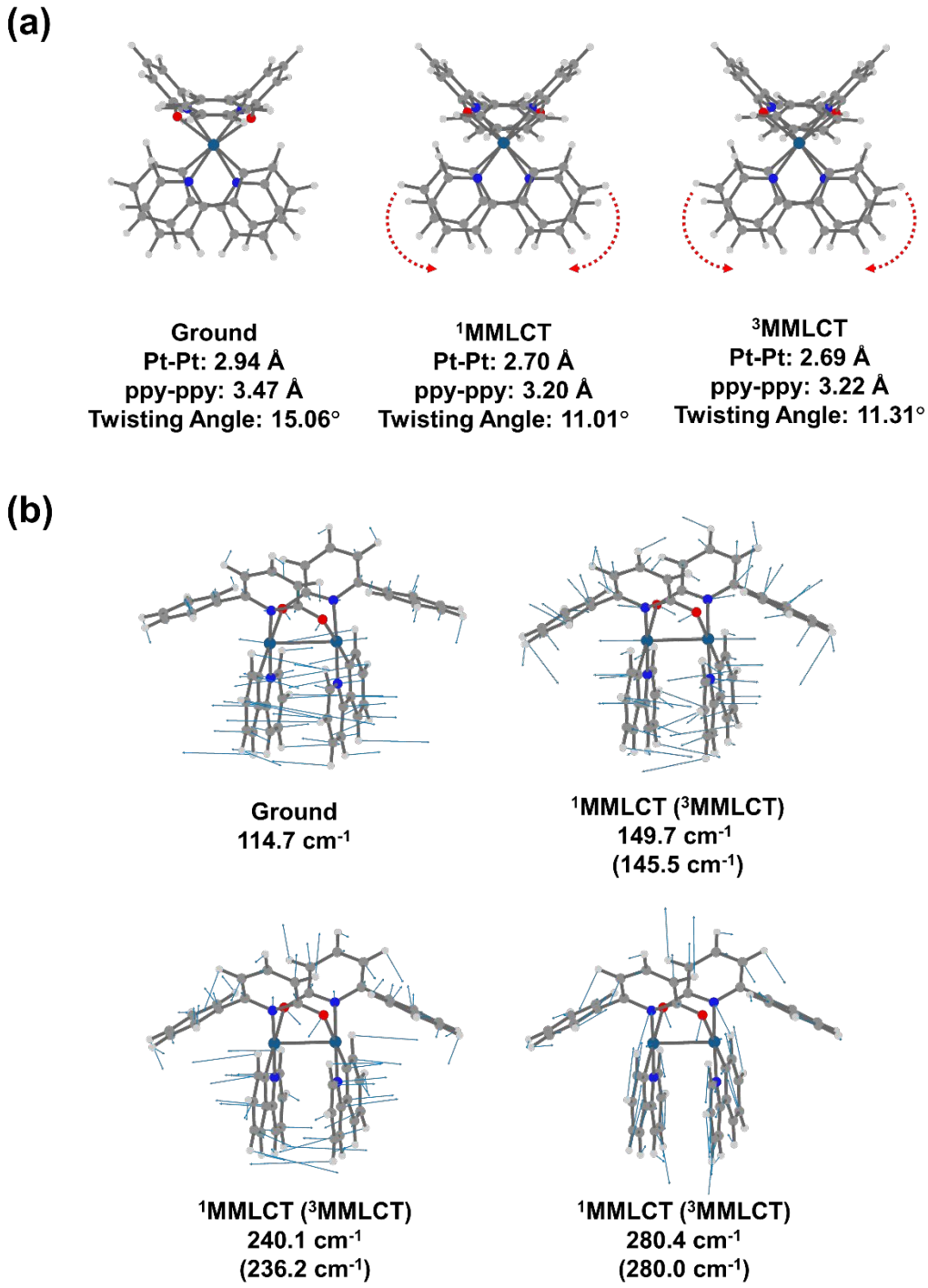

Figure 4. (a) Optimized molecular structures for ground-, ^{1}MMCLT and ^{3}MMLCT states. The red dotted arrows highlight the decrease in the twisting angle between the ppy ligand planes. (b) calculated normal modes for ground-, ^{1}MMCLT and ^{3}MMLCT states.

Pt stretching vibrational frequencies well match the observed 110 and 145 cm^{-1} CVWPs. The other normal modes around 228 and 292 cm^{-1} in the excited MMLCT states involved the interligand

vibrations oscillating parallel and perpendicular to the Pt-Pt bond axis. Therefore, as the above nuclear motions modulate the Pt-Pt distance and the distance and twisting angle between the two ligands, they can be assigned to the MMLCT active modes.

Intersystem Crossing Pathways. As depicted in Figure 5, excited-state PES calculations along the axis of Pt-Pt bond distance in our previous work proposed that the coherent Pt-Pt stretching motions can be populated in the ^{3}MMLCT state through an ultrafast ISC pathway mediated by an intermediate ^{3}LC state lying closely to the ^{1}MMLCT state.[27] The PES calculations further showed a curve crossing between the ^{1}MMLCT and the ^{3}LC states occurring in the vicinity of FC region, implying the presence of conical intersection. In the present work, the analyses of excited-state and CVWP dynamics and the normal mode calculations confirm that the short- and long-lived 145 cm^{-1} CVWPs are the coherent Pt-Pt stretching nuclear motions generated in the ^{1}MMLCT and ^{3}MMLCT states, respectively. This is consistent with our previous TA results of the same compound. However, the present BBTA measurement clearly unveiled the SE kinetics corresponding to the population dynamics of ^{1}MMLCT state. This observation demonstrates that the Pt-Pt stretching vibration in the ^{1}MMLCT state decay largely due to the ISC to the ^{3}MMLCT state. Furthermore, since the decay (1.25 ps) and damping time (~ 0.9 ps) of SE and CVWP signals are much longer than the period of 145 cm^{-1} oscillation (230 fs), the direct ISC pathway (^{1}MMLCT $\rightarrow$ ^{3}MMLCT) is impossible to transfer the coherent Pt-Pt stretching motion to the ^{3}MMLCT state. Therefore, the Pt-Pt stretching CVWP motions in the ^{3}MMLCT state is a strong indication that a fraction of the ^{1}MMLCT population branches into the ^{3}MMLCT state as fast as the period of coherent Pt-Pt stretching motion with the 145 cm^{-1} frequency.

Along this line, the 110 cm^{-1} CVWP with the damping time of ~0.2 ps captured in the present study can be strong evidence for the Pt-Pt stretching CVWP transfer occurring near the FC state. Considering the molecular orbital energy level for the Pt(II) dimer (Figure 1a), the Pt-Pt bond shrinking can regulate the dσ^* orbital energy (Figure 1a) and thus alter the MMLCT transition energy through the changes in this nuclear coordinate. As was already mentioned, if the 110 cm^{-1} CVWP is the excited-state wavepacket, its fast damping time of ~ 0.2 ps is largely due to the Pt-Pt contraction converting the Pt-Pt stretching frequency from 110 to 145 cm^{-1}. It should be noted that the TA kinetics analysis showed a decrease in the ^{1}MMLCT transition energy with a redshift of the SE feature on the similar time scale of 0.253 ps (Figure 1d). Since the energy of ^{3}LC state

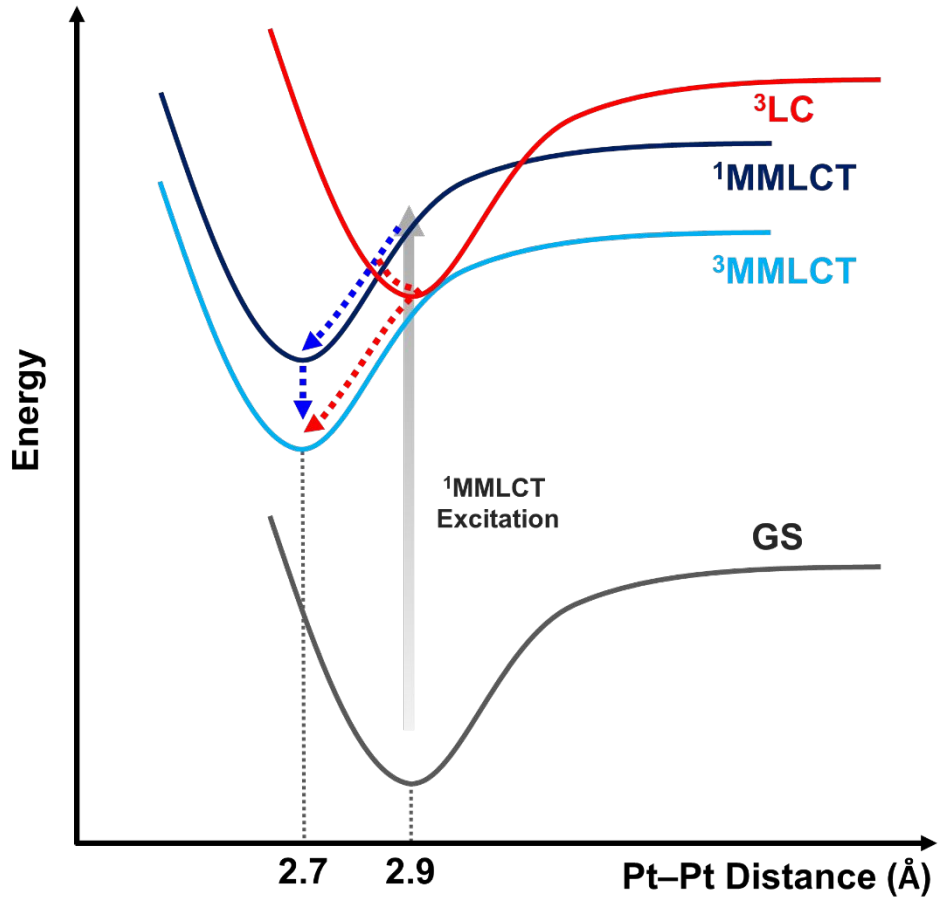

Figure 5. Schematic illustration of the excited-state PESs. The initial population of ^{1}MMLCT state branches into two ISC pathways: the direct (^{1}MMLCT → ^{3}MMLCT, blue dotted arrow) and indirect ISC path (^{1}MMLCT → ^{3}LC → ^{3}MMLCT, red dotted arrow).

is expected to be unaffected from the Pt-Pt shortening, this suggests that the Pt-Pt contraction triggered by the ^{1}MMLCT excitation moves the ^{1}MMLCT population away from the FC state and the ^{3}LC state in the early time. Therefore, it can be concluded that the ultrafast ISC and the Pt-Pt stretching CVWP transfer to the ^{3}LC state have to occur within ~ 0.2 ps before completing the Pt-Pt contraction. Although the 17.5 fs pump pulse can induce instantly the shortening of the Pt-Pt bond, the close contact between the ligands (< 3.5 Å) seems to slow down the bond contraction through the interligand structural reorganization such as the changes of distance and twisting angle between the ligand planes (Figure 4b).

Our findings shed new light on the ISC dynamics in similar bimetallic Pt(II) dimers. Recently, Mewes et al. have reported the coherent Pt-Pt stretching motions during the ISC in a pyrazolate-bridged Pt(II) dimer.[40] Interestingly, this complex has not shown the CVWP transfer to

the ^{3}MMLCT state, although the excited-state PES calculations predicted the presence of high-lying triplet state adjacent to the FC state. Furthermore, in our previous report, the CVWP transfer has not been observed in a Pt(II) dimer derivative with methyl substituents on the same bridging ligands of the present Pt(II) dimer.[27] For the Pt(II) dimer in the present study, notable structural difference from the methyl substituted Pt(II) dimer is the phenyl substituents on the bridging ligands. Even though these Pt(II) dimers have similar Pt-Pt bond length in the ground- and the excited MMLCT states, the molecular orbital calculations showed interaction between the rings and Pt(II) atoms destabilized the $d\sigma^*$ orbital, thereby lowering the ^{1}MMLCT state relative to the ^{3}LC state and then decreasing the energy gap between the FC and the ^{3}LC states more than the ones of the methyl substituted Pt(II) dimer. Therefore, close proximity in the energy between the FC and ^{3}LC states is a requirement for the ultrafast ISC and the transfer of Pt-Pt stretching CVWPs.

The TA kinetic analysis for the Pt(II) dimer is impossible to identify the transient features of the ^{3}LC state due to overlapping with the broad SE and ESA of MMLCT states. Hence, the exact time scale of the ISC pathway via the intermediate state is unknown in this work. Also, it is unclear that the Pt-Pt stretching vibrational coordinate is still the reaction coordinate for the subsequent internal conversion (IC) process from the ^{3}LC to the ^{3}MMLCT states. In the future, to prove the involvement of intermediate state and the nuclear dynamics during the IC, time-resolved impulsive stimulated Raman spectroscopy will be done to track the CVWP motions from the FC to the intermediate and then the final ^{3}MMLCT states.

Conclusion

In this work, we investigated the ISC processes from the singlet to triplet MMLCT state using the fs-BBTA spectroscopy. The ultrashort pump pulse allowed us to capture the CVWP motions associated with the photoinduced structural changes upon the ^{1}MMLCT excitation. The broadband probe spanning to 850 nm fully unraveled the SE spectral features corresponding to the ^{1}MMLCT state, which was unclear in our previous work.[27] With the aid of normal mode calculation, correlating the temporal behavior between the SE signals and the beating nodes confirmed that the short- and long-lived coherent Pt-Pt stretching vibrations with 145 cm^{-1} frequency originate from the ^{1}MMLCT and the ^{3}MMLCT states, respectively. This observation is strong indicative of ultrafast branching of the initially populated ^{1}MMLCT into the direct

(^{1}MMLCT → ^{3}MMLCT) and indirect ISC pathways (^{1}MMLCT → ^{3}LC → ^{3}MMLCT), proposed in our previous work. Furthermore, the ~ 0.2 ps vibrational dephasing of 110 cm^{-1} mode clearly resolved in the present study suggested that the branching dynamics occurs before the Pt-Pt bond contraction in order to transfer a fraction of Pt-Pt stretching CVWPs from the FC to the ^{3}LC states. This also implies that the Pt-Pt stretching motion is the key vibration for the ultrafast ISC from the ^{1}MMLCT to ^{3}LC states. In conclusion, comprehensive interrogation of vibrational wavepacket dynamics provides new insight into the impact of the photoinduced Pt-Pt contraction on the ISC processes in the Pt(II) dimer. We believe that the methodology used to evaluate the vibrational wavepacket evolution in our study can contribute to a better understanding of ultrafast excited-state and structural dynamics for other TMCs.

Conflicts of Interest

There are no conflicts to declare.

Acknowledgements

This work has been supported by the National Science Foundation (CHE-1955806 to LXC and CHE-1955795 to FNC). The computational work and P.K. and L.X.C. are supported in part by the Ultrafast Initiative of the U. S. Department of Energy, Office of Science, Office of Basic Energy Sciences, through Argonne National Laboratory under Contract No. DE-AC02-06CH11357. The development of computational method for simulating excited state dynamics is supported by the National Science Foundation (CHE-1856210 to XL).

References

1. J. K. McCusker, *Science*, 2019, **363**, 484.
2. M. W. Mara, D. N. Bowman, O. Buyukcakir, M. L. Shelby, K. Haldrup, J. Huang, M. R. Harpham, A. B. Stickrath, X. Zhang, J. F. Stoddart, A. Coskun, E. Jakubikova and L. X. Chen, *Journal of the American Chemical Society*, 2015, **137**, 9670-9684.
3. T. C. B. Harlang, Y. Liu, O. Gordivska, L. A. Fredin, C. S. Ponseca, P. Huang, P. Chábera, K. S. Kjaer, H. Mateos, J. Uhlig, R. Lomoth, R. Wallenberg, S. Styring, P. Persson, V. Sundström and K. Wärnmark, *Nature Chemistry*, 2015, **7**, 883-889.

4. J. Twilton, C. Le, P. Zhang, M. H. Shaw, R. W. Evans and D. W. C. MacMillan, *Nature Reviews Chemistry*, 2017, **1**, 0052.
5. D. M. Arias-Rotondo and J. K. McCusker, *Chemical Society Reviews*, 2016, **45**, 5803-5820.
6. O. S. Wenger, *Journal of the American Chemical Society*, 2018, **140**, 13522-13533.
7. K. Kalyanasundaram and M. Grätzel, *Coordination Chemistry Reviews*, 1998, **177**, 347-414.
8. M. Chaaban, C. Zhou, H. Lin, B. Chyi and B. Ma, *Journal of Materials Chemistry C*, 2019, **7**, 5910-5924.
9. N. Huse, T. K. Kim, L. Jamula, J. K. McCusker, F. M. F. de Groot and R. W. Schoenlein, *Journal of the American Chemical Society*, 2010, **132**, 6809-6816.
10. W. Zhang, R. Alonso-Mori, U. Bergmann, C. Bressler, M. Chollet, A. Galler, W. Gawelda, R. G. Hadt, R. W. Hartsock, T. Kroll, K. S. Kjær, K. Kubiček, H. T. Lemke, H. W. Liang, D. A. Meyer, M. M. Nielsen, C. Purser, J. S. Robinson, E. I. Solomon, Z. Sun, D. Sokaras, T. B. van Driel, G. Vankó, T.-C. Weng, D. Zhu and K. J. Gaffney, *Nature*, 2014, **509**, 345-348.
11. H. T. Lemke, K. S. Kjær, R. Hartsock, T. B. van Driel, M. Chollet, J. M. Glownia, S. Song, D. Zhu, E. Pace, S. F. Matar, M. M. Nielsen, M. Benfatto, K. J. Gaffney, E. Collet and M. Cammarata, *Nature Communications*, 2017, **8**, 15342.
12. T. Katayama, T. Northey, W. Gawelda, C. J. Milne, G. Vankó, F. A. Lima, R. Bohinc, Z. Németh, S. Nozawa, T. Sato, D. Khakhulin, J. Szlachetko, T. Togashi, S. Owada, S.-i. Adachi, C. Bressler, M. Yabashi and T. J. Penfold, *Nature Communications*, 2019, **10**, 3606.
13. S. Cho, M. W. Mara, X. Wang, J. V. Lockard, A. A. Rachford, F. N. Castellano and L. X. Chen, *The Journal of Physical Chemistry A*, 2011, **115**, 3990-3996.
14. M. Iwamura, S. Takeuchi and T. Tahara, *Accounts of Chemical Research*, 2015, **48**, 782-791.
15. G. Auböck and M. Chergui, *Nature Chemistry*, 2015, **7**, 629-633.
16. J. D. Gaynor, J. Sandwisch and M. Khalil, *Nature Communications*, 2019, **10**, 5621.
17. Q.-C. Zhang, H. Xiao, X. Zhang, L.-J. Xu and Z.-N. Chen, *Coordination Chemistry Reviews*, 2019, **378**, 121-133.
18. B. Ma, J. Li, P. I. Djurovich, M. Yousufuddin, R. Bau and M. E. Thompson, *Journal of the American Chemical Society*, 2005, **127**, 28-29.
19. A. A. Rachford and F. N. Castellano, *Inorganic Chemistry*, 2009, **48**, 10865-10867.
20. A. Chakraborty, J. C. Deaton, A. Haefele and F. N. Castellano, *Organometallics*, 2013, **32**, 3819-3829.
21. M. Han, Y. Tian, Z. Yuan, L. Zhu and B. Ma, *Angewandte Chemie International Edition*, 2014, **53**, 10908-10912.
22. C. Zhou, L. Yuan, Z. Yuan, N. K. Doyle, T. Dilbeck, D. Bahadur, S. Ramakrishnan, A. Dearden, C. Huang and B. Ma, *Inorganic Chemistry*, 2016, **55**, 8564-8569.
23. S. E. Brown-Xu, M. S. J. Kelley, K. A. Fransted, A. Chakraborty, G. C. Schatz, F. N. Castellano and L. X. Chen, *The Journal of Physical Chemistry A*, 2016, **120**, 543-550.
24. J. V. Lockard, A. A. Rachford, G. Smolentsev, A. B. Stickrath, X. Wang, X. Zhang, K. Atenkoffer, G. Jennings, A. Soldatov, A. L. Rheingold, F. N. Castellano and L. X. Chen, *The Journal of Physical Chemistry A*, 2010, **114**, 12780-12787.
25. K. Haldrup, A. O. Dohn, M. L. Shelby, M. W. Mara, A. B. Stickrath, M. R. Harpham, J. Huang, X. Zhang, K. B. Møller, A. Chakraborty, F. N. Castellano, D. M. Tiede and L. X. Chen, *The Journal of Physical Chemistry A*, 2016, **120**, 7475-7483.
26. P. Kim, M. S. Kelley, A. Chakraborty, N. L. Wong, R. P. Van Duyne, G. C. Schatz, F. N. Castellano and L. X. Chen, *The Journal of Physical Chemistry C*, 2018, **122**, 14195-14204.
27. P. Kim, A. J. S. Valentine, S. Roy, A. W. Mills, A. Chakraborty, F. N. Castellano, X. Li and L. X. Chen, *The Journal of Physical Chemistry Letters*, 2021, **12**, 6794-6803.

28. A. Chakraborty, J. E. Yarnell, R. D. Sommer, S. Roy and F. N. Castellano, *Inorganic Chemistry*, 2018, **57**, 1298-1310.
29. A. Grupp, A. Budweg, M. P. Fischer, J. Allerbeck, G. Soavi, A. Leitenstorfer and D. Brida, *Journal of Optics*, 2017, **20**, 014005.
30. M. J. Frisch, G. W. Trucks, H. B. Schlegel, G. E. Scuseria, M. A. Robb, J. R. Cheeseman, G. Scalmani, V. Barone, G. A. Petersson, H. Nakatsuji, X. Li, M. Caricato, A. V. Marenich, J. Bloino, B. G. Janesko, R. Gomperts, B. Mennucci, H. P. Hratchian, J. V. Ortiz, A. F. Izmaylov, J. L. Sonnenberg, Williams, F. Ding, F. Lipparini, F. Egidi, J. Goings, B. Peng, A. Petrone, T. Henderson, D. Ranasinghe, V. G. Zakrzewski, J. Gao, N. Rega, G. Zheng, W. Liang, M. Hada, M. Ehara, K. Toyota, R. Fukuda, J. Hasegawa, M. Ishida, T. Nakajima, Y. Honda, O. Kitao, H. Nakai, T. Vreven, K. Throssell, J. A. Montgomery Jr., J. E. Peralta, F. Ogliaro, M. J. Bearpark, J. J. Heyd, E. N. Brothers, K. N. Kudin, V. N. Staroverov, T. A. Keith, R. Kobayashi, J. Normand, K. Raghavachari, A. P. Rendell, J. C. Burant, S. S. Iyengar, J. Tomasi, M. Cossi, J. M. Millam, M. Klene, C. Adamo, R. Cammi, J. W. Ochterski, R. L. Martin, K. Morokuma, O. Farkas, J. B. Foresman and D. J. Fox, *Journal*, 2016.
31. P. J. Hay and W. R. Wadt, *The Journal of Chemical Physics*, 1985, **82**, 299-310.
32. J.-D. Chai and M. Head-Gordon, *Physical Chemistry Chemical Physics*, 2008, **10**, 6615-6620.
33. A. J. Atkins, F. Talotta, L. Freitag, M. Boggio-Pasqua and L. González, *Journal of Chemical Theory and Computation*, 2017, **13**, 4123-4145.
34. J. J. Snellenburg, S. P. Laptenok, R. Seger, K. M. Mullen and I. H. M. van Stokkum, *Journal of Statistical Software*, 2012, **49**, 1-22.
35. H. F. Shurvell and M. C. Southby, *Vibrational Spectroscopy*, 1997, **15**, 137-146.
36. M. H. Vos, F. Rappaport, J.-C. Lambry, J. Breton and J.-L. Martin, *Nature*, 1993, **363**, 320-325.
37. S. D. McClure, D. B. Turner, P. C. Arpin, T. Mirkovic and G. D. Scholes, *The Journal of Physical Chemistry B*, 2014, **118**, 1296-1308.
38. C. C. Jumper, P. C. Arpin, D. B. Turner, S. D. McClure, S. Rafiq, J. C. Dean, J. A. Cina, P. A. Kovac, T. Mirkovic and G. D. Scholes, *The Journal of Physical Chemistry Letters*, 2016, **7**, 4722-4731.
39. S. Rafiq and G. D. Scholes, *The Journal of Physical Chemistry A*, 2016, **120**, 6792-6799.
40. L. Mewes, R. A. Ingle, S. Megow, H. Böhnke, E. Baranoff, F. Temps and M. Chergui, *Inorganic Chemistry*, 2020, **59**, 14643-14653.
41. N. P. Weingartz, M. W. Mara, S. Roy, J. Hong, A. Chakraborty, S. E. Brown-Xu, B. T. Phelan, F. N. Castellano and L. X. Chen, *The Journal of Physical Chemistry A*, 2021, **125**, 8891-8898.